Національна академія наук України

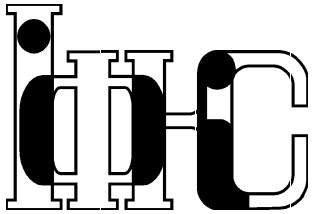

ІНСТИТУТ ФІЗИКИ КОНДЕНСОВАНИХ СИСТЕМ

ICMP–24–04E

T. Hutak, J. Richter*, T. Krokhmalskii, O. Derzhko

PRELIMINARIES ON THERMODYNAMICS
OF THE SPIN-S HEISENBERG ANTIFERROMAGNET
ON THE KAGOME LATTICE

*Institut für Physik, Otto-von-Guericke-Universität Magdeburg,
P.O. Box 4120, 39016 Magdeburg, Germany

ЛЬВІВ

УДК: 537.9; 537.622

PACS: 75.10.-b

Попередні результати стосовно термодинаміки спін-S антиферомагнетика Гайзенберга на гратці кагоме

Т. Гутак, Й. Ріхтер, Т. Крохмальський, О. Держко

Анотація. Ми використовуємо високотемпературні розвинення за степенями оберненої температури $\beta = 1/T$ до 11 порядку і метод ентропії щоб обчислити магнітну теплоємність $c(T)$ та магнітну однорідну сприйнятливість $\chi(T)$ для антиферомагнетика Гайзенберга зі спіном $S > 1/2$ на гратці кагоме. Ми доповнюємо ці обчислення даними методу точної діагоналізації і скінченотемпературного методу Ланцоша для скінчених систем. Ми обговорюємо як змінюється температурна залежність теплоємності із ростом спінового квантового числа S.

Preliminaries on thermodynamics of the spin-S Heisenberg antiferromagnet on the kagome lattice

T. Hutak, J. Richter, T. Krokhmalskii, O. Derzhko

Abstract. We use high-temperature expansion series up to order 11 in the inverse temperature $\beta = 1/T$ and the entropy method to calculate the magnetic specific heat $c(T)$ and the magnetic uniform susceptibility $\chi(T)$ for the kagome-lattice Heisenberg antiferromagnet with spin $S > 1/2$. We complement these calculations by exact diagonalization and finite-temperature Lanczos method data for finite systems. We discuss how the temperature dependence of the specific heat varies as the spin quantum number S grows.

Препринти Інституту фізики конденсованих систем НАН України розповсюджуються серед наукових та інформаційних установ. Вони також доступні по електронній комп'ютерній мережі на WWW-сервері інституту за адресою http://www.icmp.lviv.ua/

The preprints of the Institute for Condensed Matter Physics of the National Academy of Sciences of Ukraine are distributed to scientific and informational institutions. They also are available by computer network from Institute's WWW server (http://www.icmp.lviv.ua/)

Тарас Ігорович Гутак
Йоганес Ріхтер
Тарас Євстахійович Крохмальський
Олег Володимирович Держко

Попередні результати стосовно термодинаміки спін-S антиферомагнетика Гайзенберга на гратці кагоме

Роботу отримано 2 грудня 2024 р.

Затверджено до друку Вченою радою ІФКС НАН України

Рекомендовано до друку відділом квантової статистики

Виготовлено при ІФКС НАН України

1. Introduction

The spin-S Heisenberg model with the antiferromagnetic nearest-neighbor exchange coupling $J > 0$ (usually, $J = 1$) on the kagome lattice (KHAF) is a paradigmatic model in frustrated quantum magnetism, which attracts a lot of attention both from theoretical and experimental sides [1]. The spin value $S = 1/2$ represents the pure quantum case, whereas $S \to \infty$ corresponds to the classical case. Thus, the spin value S controls the role of quantum fluctuations which together with geometrical frustration and thermal fluctuations are known to produce intriguing properties of such a spin-lattice system. In what follows, we intend to illustrate how some temperature characteristics of the KHAF depend on S. Before that we briefly recall what is needed for our study.

Concerning the ground-state properties, it is believed that the ground state of the $S = 1/2$ KHAF is a gapless spin liquid. However, there are several gapless spin-liquid states, which distinguish by a law for the specific heat decay as $T \to 0$.

The ground-state physics of the $S = 1$ KHAF has been in focus of many papers [2–16]. Various proposals have been suggested for the ground state. Thus, Hida proposed a hexagon-singlet solid (HSS) state as a candidate ground state [2]. An alternative candidate is the resonating Affleck-Kennedy-Lieb-Tasaki loop (RAL) state [6]. Another plausible ground state, which although nonmagnetic but breaks lattice inversion symmetry and possesses a simplex valence-bond crystal (SVBC) order, is the SVBC state which favors trimerization [4, 7, 8, 10]. The ground-state energy (per site) calculated by various methods can be found in Supplemental Material. Most of data lie around $-1.41\ldots-1.40$. Furthermore, the $S = 1$ KHAF is expected to be gapped. That is, in contrast to the $S = 1/2$ case, the nonmagnetic excitations have finite energy gap comparable to the one for the magnetic excitations. The value of the spin gap is estimated in the range $0.2 - 0.3$ [10]. The DMRG calculations of Ref. [13] give the following estimates for the singlet-triplet gap Δ_{s-t}: 0.178 ± 0.005 for the HSS state and 0.2797 for the (triangular valence-bond solid) TVBS state.

The ground-state energy for the $S = 3/2$ KHAF can be found in Supplemental Material. For $S \geq 3/2$ a ground-state magnetic long-range order may appear [5, 9, 15, 17]. It was argued that the $\sqrt{3} \times \sqrt{3}$ state is the ground state which melts at any finite temperature [17].

Classical ($S \to \infty$) ground states were discussed in Ref. [18]. The set of all ground states is disordered, but as $T \to 0$, however, the entropy of fluctuations select a nematic correlations.

Concerning the finite-temperature properties of the $S = 1/2$ KHAF, an extra low-temperature peak or shoulder in the magnetic specific heat at the temperature about ten times smaller than J is debated [19–29]. Moreover, an enhanced magnetic susceptibility at low temperatures below half of J was observed [27, 30].

For $S = 3/2$, the specific heat exhibits a T^2 behavior and the susceptibility approaches a finite constant as $T \to 0$ [17].

For the classical case $S \to \infty$, it is known that the specific heat with temperature decrease exhibits a maximum before achieves the value $11/12$ at $T = 0$ [18]. In connection with the susceptibility, we note that it reaches the value $\chi_0 = 1/6$ as temperature goes to zero [31, 32].

Concerning experiments, high quality crystals of herbertsmithite $ZnCu_3(OH)_6Cl_2$, in which the copper ions carrying spin one-half sit on a kagome lattice, were synthesized in 2005. Much more $S = 1/2$ KHAF realistic materials are known nowadays. This motivates an interest in the theoretical study of the $S = 1/2$ KHAF: It would be highly desirable to compare experiments with theory [33–35]. However, for a precise explanation of finite-temperature measurements it is necessary to explore side effects unavoidably present in real crystals. Thus, disorder (as nonmagnetic impurities) and several extra interactions for the $S = 1/2$ case were discussed in detail using the entropy method by Bernu *et al.* [29].

Although, various magnetic kagome compounds with $S > 1/2$ exist, see, e.g., Refs. [36–47] for $S = 1$ and Refs. [48–52] for higher S, much less corresponding theoretical work is available. While for the ground state several recent studies for $S > 1/2$ exist [2–16], only a few theoretical investigations of finite-temperature properties of the KHAF are known [17, 53].

In what follows, we study the thermodynamics of the spin-S KHAF focusing on the specific heat $c(T)$ and the susceptibility $\chi(T)$. Theoretical methods to study thermodynamics of highly frustrated quantum Heisenberg antiferromagnets are rather scarce. Thus, quantum Monte Carlo simulations are inapplicable because of the sign problem, exact diagonalization and finite-temperature Lanczos methods are limited to relatively small system sizes N [27, 54, 55], which become even smaller when $S > 1/2$, the numerical linked-cluster approach to quantum lattice models cannot access sufficiently low temperatures [24, 25], whereas the second-order rotation-invariant Green's-function method (RGM) is too crude to reveal fine low-temperature features [53]. Furthermore, a raw high-temperature expansion being complemented by Padé approximants is restricted to the temperature range above $\sim 0.5J$. Here we use the entropy-method interpolation for thermodynamically large systems.

The key element of the entropy method is a sophisticated procedure of interpolation between the known low- and high-temperature properties in the microcanonical ensemble which respect the sum rules constraining the specific heat [23, 29, 56–63]. Besides, we complement the entropy-method results by numerical calculations for finite-size systems. Our aim is to follow how the thermodynamic properties vary as the spin value increases from the pure quantum limit $S = 1/2$ to the classical limit $S \to \infty$.

We end up this section with introducing the model and notations. We consider the kagome-lattice Heisenberg antiferromagnet with the Hamiltonian

$$H = \sum_{\langle nm \rangle} \boldsymbol{S}_n \cdot \boldsymbol{S}_m. \tag{1}$$

Here the antiferromagnetic exchange coupling $J > 0$ is set to unity, the sum runs over nearest-neighbor bonds on the kagome lattice, and $\boldsymbol{S}_n^2 = S(S+1)$, $S = 1/2, 1, 3/2, \ldots$ (in what follows, the largest value of S is 4). We set $\hbar = 1$ and $k_B = 1$ throughout the paper.

In the rest of the paper, we first concisely explain the exploited methods (Section 2) and then report the obtained results (Section 3). We end up with a brief summary (Section 4).

2. Methods

The main method of our study is the high-temperature expansion (HTE) augmented further by the entropy-method interpolation which was elaborated for thermodynamically large spin systems without a finite-temperature phase transition in Refs. [23, 29, 56, 57]. First, we use the HTE program of Refs. [64, 65], which is freely available at

`http://www.uni-magdeburg.de/jschulen/HTE/`,

in an extended version up to nth order ($n = 13$ for $S = 1/2$ and $n = 11$ for $S > 1/2$). Thus, we compute the series of the specific heat (per site) $c(T) = \sum_{i=2}^{n} d_i \beta^i + \mathcal{O}(\beta^{n+1})$ ($d_1 = 0$) and the static uniform susceptibility (per site) $\chi(T) = \sum_{i=1}^{n} c_i \beta^i + \mathcal{O}(\beta^{n+1})$ with respect to the inverse temperature $\beta = 1/T$. (Recently, an algorithm for calculating high-temperature expansion series of Heisenberg models in the thermodynamic limit, which accounts for the presence of a magnetic field, has been reported [66]; however, this algorithm is restricted to the spin value $S = 1/2$.) As a result, we have the following high-temperature series for

the Helmholtz free energy (per site) for low magnetic fields h ($g\mu_{\rm B}=1$)

$$-\beta f(T,h)=\frac{\ln Z(\beta,h,N)}{N}$$
$$\stackrel{\beta\to 0}{=}\ln(2S+1)+\sum_{i=2}^{n}\frac{d_i}{(i-1)i}\beta^i+\mathcal{O}(\beta^{n+1})$$
$$+\frac{1}{2}\beta\left(\sum_{i=1}^{n}c_i\beta^i+\mathcal{O}(\beta^{n+1})\right)h^2+\mathcal{O}(h^4), \qquad (2)$$

where $Z(\beta,h,N)$ is the canonical partition function. HTE up to 10th order for arbitrary spin S can be found in Appendix B of Ref. [65]. In the present paper, we use one more order results, that is,

$$d_{11}=-\frac{76\,377\,321\,757}{66\,134\,880}J^{11},\quad c_{11}=\frac{49\,904\,041}{47\,239\,200}J^{10} \qquad (3)$$

for $S=1$,

$$d_{11}=-\frac{6\,245\,386\,099\,381}{24\,772\,608}J^{11},\quad c_{11}=\frac{12\,298\,193\,957}{2\,211\,840}J^{10} \qquad (4)$$

for $S=3/2$; d_{11} and c_{11} for $S=2$, 5/2, 3, 7/2, and 4 can be found in Supplemental Material.

The most straightforward way to extend the region of validity of the raw HTE is to construct simple Padé approximants [65]. Our studies on the spin-S KHAF used HTE up to 11th order. Therefore, we may construct $[u,d](T)$, $u+d\le n=11$ and in what follows we show the close to diagonal Padé approximants like $[4,5](T)$, $[4,6](T)$, $[5,5](T)$, $[6,4](T)$, $[5,6](T)$, $[6,5](T)$.

As a key tool, we exploit the entropy method [23, 29, 56, 57] to interpolate between the high-temperature behavior given by the HTE and the presumed low-temperature behavior to get thermodynamic quantities over the full temperature range. This procedure is explained for self consistency in Supplemental Material. Here we only mention that we work in the microcanonical ensemble with the entropy (per site) as a function of the internal energy (per site) $s(e)$. We need, besides the known Maclaurin series for $s(e)$ up to order $n=11$, the ground-state energy per site e_0 and the behavior of the specific heat $c(T)$ as $T\to 0$, which determines $s(e)$ as $e\to e_0{+}0$. Then we interpolate an auxiliary function $G(e)$, which depends on the specific low-temperature behavior of $c(T)$ and which is uniquely related to $s(e)$, using (two-point like) Padé approximants $[u,d](e)$, $u+d\le n=11$. According to Ref. [29], if e_0 is exact, the adopted low-temperature $c(T)$ is correct, and n is sufficiently large, the approximate entropy-method $c_{\rm app}(T)$ for all $[u,d](e)$ is close to the exact one[1]. The described prescription can be straightforwardly extended in the presence of a magnetic field to obtain the susceptibility $\chi(T)$, however, $\chi_0\equiv\chi(T{=}0)$ is necessary as an extra input parameter if the low-energy excitations are gapless. We are not aware about χ_0 for $S=3/2$, 2, 5/2, 3, 7/2, 4 besides RGM data [53] which, however, are not enough accurate to be used for interpolation.

A complementary method of our study is the exact diagonalization and the finite-temperature Lanczos methods which allow to illustrate the temperature dependences $c(T)$ and $\chi(T)$ for the finite-size $S=1$ KHAF. The clusters with $N=18$, 21 and periodic boundary conditions imposed are used to obtain $c(T)$ and $\chi(T)$. Finite-temperature Lanczos method is explained in some detail in Ref. [27]. Within its frames, the sum in the partition function over all states within the Hilbert space of the model is replaced by the sum over R different randomly chosen states. In our study we used $R=10\ldots200$ to balance the accuracy and the required computation time.

3. Results

First, we discuss in some detail the case $S=1$ KHAF, which has been considered in several recent papers. Then we pass to the case of higher spin values $S=3/2$, 2, 5/2, 3, 7/2, 4, which is less studied.

3.1. $S=1$

We begin with numerics for finite-size systems, see Fig. 1. Several observations are immediately evident. The results for different numbers of sites coincide above the temperature approximately equals 0.7 for $c(T)$ or 0.5 for $\chi(T)$ indicating the confidence region. Next, $c(T)$ has a low-temperature maximum, the position of which lies outside the confidence region and is size-dependent (≈ 0.17 for $N=18$ but ≈ 0.11 for $N=21$). $\chi(T)$ illustrates a gapped spectrum (although a finite system is always gapped), but the position of maximum (≈ 0.44 for $N=18$ and ≈ 0.40 for $N=21$) is outside the confidence region. Finally, having only two values $N=18$ and $N=21$ it is impossible to predict low-temperature behavior of c and χ as $N\to\infty$, and thus numerics is inconclusive even for the $S=1$ case.

[1] This observation can be used to proceed even in the case when the ground state and low-energy excitations are unknown [29, 63].

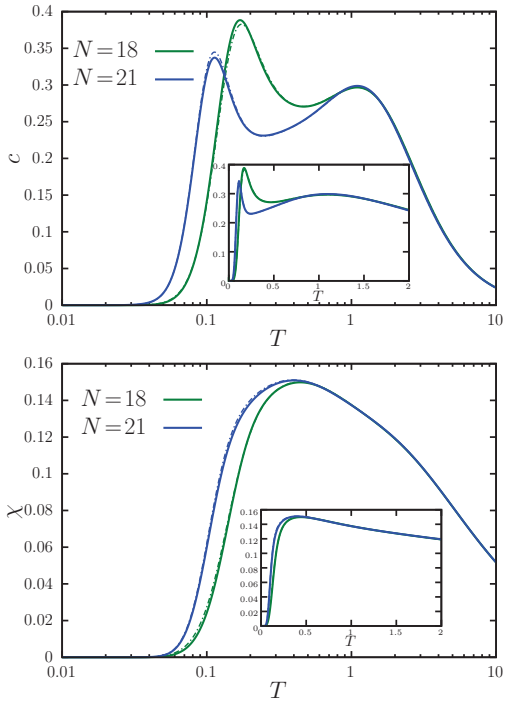

Figure 1. Numerics for (top) $c(T)$ and (bottom) $\chi(T)$ of the $S = 1$ KHAF of $N = 18$ (green) and $N = 21$ (blue) sites. Solid and dash-dotted lines correspond to $R = 200$ ($N = 18$), $R = 50$ ($N = 21$) and $R = 100$ ($N = 18$), $R = 10$ ($N = 21$), respectively, see Sec. 2. The insets present the same data in linear scale. The results for different sizes practically coincide above 0.7 for $c(T)$ and 0.5 for $\chi(T)$.

We pass to the entropy-method calculations. As said above, HTE series up to 11th order (Ref. [65] and Eq. (3)) for the model at hand is available. Furthermore, the required low-temperature properties are known: We may take for the ground-state energy, e.g., $e_0 = -1.41$, see Supplemental Material, and assume gapped excitations.

In Fig. 2 we report the entropy-method results (along with simple Padé extrapolations and numerics) for $c(T)$ and $\chi(T)$ of the $S = 1$ KHAF. As can be seen in the top panel of Fig. 2, the entropy-method curves agree with simple Padé approximants and numerics in the high-temperature region. Above that, $c(T)$ exhibits a shoulder in the temper-

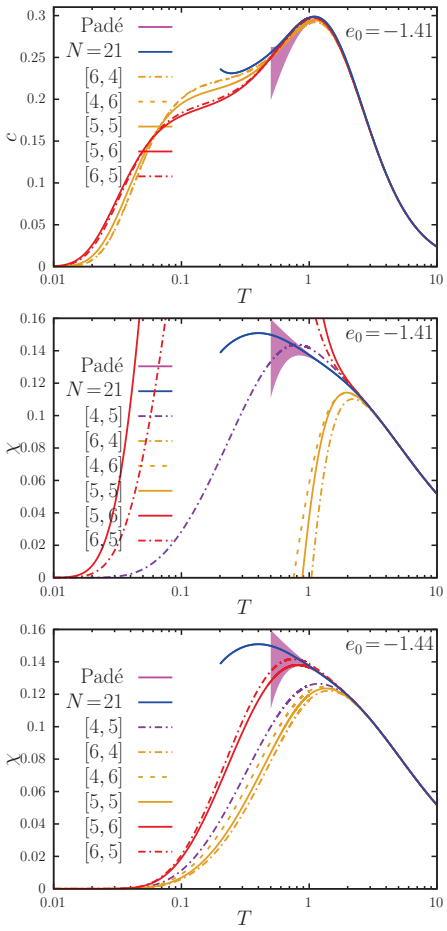

Figure 2. Entropy-method results (red, gold, violet) along with simple Padé (magenta) and finite-size (blue) data for (top) $c(T)$ and (middle and bottom) $\chi(T)$ of the $S = 1$ KHAF. Entropy-method curves based on $[5,6](e)$, $[6,5](e)$, $[4,6](e)$, $[5,5](e)$, $[6,4](e)$, and also on $[4,5](e)$ for $\chi(T)$ with (top and middle) $e_0 = 1.41$ and (bottom) $e_0 = -1.44$, simple Padé approximants, $[5,6](T)$ and $[6,5](T)$, and the shaded region between them are shown for $T \geq 0.5$, whereas numerics for $N = 21$ are shown for $T \geq 0.2$. Note that simple Padé approximants and numerics can reproduce the main maximum of $c(T)$ but not a shoulder below it. Furthermore, the maximum of $\chi(T)$ is predicted differently by different approaches.

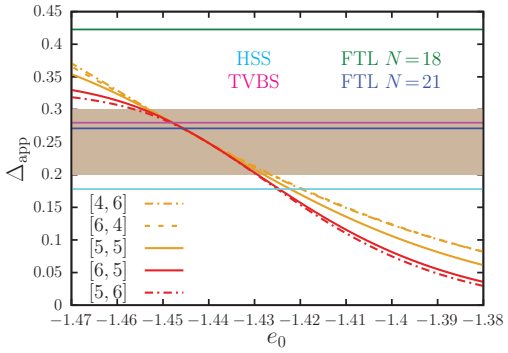

Figure 3. Entropy-method results (red, gold) for the energy gap Δ of the $S = 1$ KHAF. We also show results for finite systems, of DMRG calculations (gray stripe) [10], as well as results under the hypothesis of HSS or TVBS ground state [13].

ature range $0.07 - 0.3$. Recall that for the $S = 1/2$ KHAF, the entropy-method calculations under both assumptions, of gapless spectrum with $\alpha = 1$, 2 [23] or of gapped one [57], yield an extra low-temperature maximum of $c(T)$. In the middle panel of Fig. 2 we report $\chi(T)$ for the $S = 1$ KHAF as it follows from the entropy-method interpolation ($e_0 = -1.41$, gapped exciations) along with simple Padé approximations and numerics. Obviously, the agreement between various entropy-method curves is rather poor (essentially worse in comparison to the case of specific heat) and only one of them, which is based of $[4, 5](e)$, yields a plausible profile of $\chi(T)$ (maximum around 0.80 of the height about 0.14). We note that decreasing the ground-state energy e_0 from the value -1.41 to the value -1.44, i.e., by 2.1%, leads to better agreement between various entropy-method curves (more Padé approximants are closer to each other), see the bottom panel of Fig. 2. One may speculate that having only $n = 11$ coefficients of high-temperature expansion series one gets a relatively self-consistent entropy-method prediction for $\chi(T)$ if the assumed e_0 is 102.1% of the true ground-state energy ≈ -1.41, but with further increasing n the assumed value e_0 will tend to the true value $e_0 \approx -1.41$.

To gain more insight into this problem, we discuss an energy gap of the $S = 1$ KHAF. In Fig. 3 we show the dependence of the entropy-method gap Δ as a function of the assumed ground-state energy e_0. Setting $e_0 = -1.41$, we get the gap value within the range $[0.11, 0.15]$.

Furthermore, we report in Fig. 3 the singlet-triplet (magnetic or spin) gap according to DMRG calculations, which lies in the range between 0.2 and 0.3 [10] along with the expected gaps for HSS and TVBS ground states [13]. As it follows from Fig. 3, the entropy-method $\Delta = 0.2$ appears if $e_0 \approx -1.43$. It is important to note that the entropy method does not distinguish the singlet-singlet gap and the singlet-triplet gap and yield the value of the lowest-energy gap, which governs the low-temperature behavior of the specific heat. Therefore, the entropy method may face a problem if the singlet-singlet (nonmagnetic) gap is smaller than the singlet-triplet gap: The former gap follows from the entropy-method calculations but the latter one, which is larger and not present in the entropy-method scheme, controls the low-temperature behavior of the susceptibility. If for the case under consideration Δ_{s-s} is smaller than Δ_{s-t}, see above, it is not astonishing that the entropy-method output for $\chi(T)$ is worse than for $c(T)$. Decrease of e_0 results in increase of the energy gap, see Fig. 3, and might improve the entropy-method output for $\chi(T)$. However, the problems with $\chi(T)$ within the entropy method may be more intricate as is illustrated for the square-lattice $S = 1/2$ and $S = 1$ Heisenberg antiferromagnet in Supplemental Material.

To summarize this subsection, neither numerics no simple Padé approximants can reproduce $c(T)$ and $\chi(T)$ below $T = 0.5$. Although the entropy-method interpolation contains correct low-temperature behavior of the model at hand, because of only $n = 11$ terms of HTE available and "worse" HTE series for $S > 1/2$, it can reproduce temperature profiles only modestly in comparison to the $S = 1/2$ case (less almost coinciding Padé approximants). Moreover, the results for the specific heat look better than the ones for the susceptibility which may be related to singlet (nonmagnetic) lowest-energy excitations above the gapped ground state.

3.2. $S > 1$

Bearing in mind the results for the $S = 1/2$ KHAF [23, 29, 57] and for the $S = 1$ KHAF (see previous subsection), we pass to the cases $S = 3/2$, 2, 5/2, 3, 7/2, 4. Since the ground state for $S \geq 3/2$ possesses a magnetic long-range order, it seems reasonable to assume the gapless spectrum with $\alpha = 2$ for all $S \geq 3/2$. The values of e_0 are available from the coupled cluster method (CCM) calculations [5], whereas the values of χ_0 may be taken, in principle, from the RGM calculations [53]. However, in view of that the RGM approach is not precise enough and the entropy method faces some difficulties in obtaining $\chi(T)$ for gapples excitations too (see Supplemental Material), we restrict ourselves in what follows to $c(T)$ only. Before presenting our findings, it might be worth to recall that

(i) $S = 3/2$ results were reported in Ref. [17] (but the curve $c(T)$ reported there hardly obey the sum rule $\int_0^\infty \mathrm{d}T c(T)/T = \ln(2S+1)$, see Fig. 4) and (ii) a number of reliable classical Monte Carlo simulations data for $c(T)$ and $\chi(T)$ for the case $S \to \infty$ were reported in Refs. [18, 31, 32, 67].

In Fig. 4 we show entropy-method curves $c(T)$ for the cases $S = 3/2$, $S = 2$, and $S = 5/2$. Some of Padé approximants $[u, d](e)$ are with "defects" (see Ref. [68], pp. 38-66) and must be put in the proper perspective, see Refs. [62, 68]. Following the temperature profiles $c(T)$ obtained on the basis of $[5, 6](e)$, $[6, 5](e)$, and $[5, 5](e)$, one may conclude that the low-temperature shoulder fades away as the spin value S exceeds $S = 2$. (Note, however, that such a behavior holds for the 11th order results; the 10th and 9th orders lead to a rather dispersive bunch of curves $c(T)$.) Below, we consider the 11th order Padé approximant $[5, 6](e)$ only to continue discussion of the spin value effect on $c(T)$.

In the top panel of Fig. 5 we report $c(T)$ for several spin values $S = 1/2$, 1, $3/2$, 2, $5/2$, 3, $7/2$, 4 and $S \to \infty$ to demonstrate how the pure quantum case ($S = 1/2$) transforms into the classical one ($S \to \infty$). As can be seen from this figure, there are some hints for low-temperature features (peak or shoulder) if $S = 1/2,\ 1,\ 3/2$; the case $S = 2$ is marginal; and there is only one peak in $c(T)$ if $S = 5/2$, 3, $7/2$, 4. In the bottom panel of Fig. 5, we illustrate how the main peak in the specific heat $c_{\max} = c(T_{\max})$ is modified as S varies. Namely, we report the dependence of the height of the main maximum $c_{\max}$ (main panel) and its position $T_{\max}$ (inset) as functions of the spin value S. We present results of different methods: Entropy method, simple Padé approximation, numerics. Again the spin value $S = 2$ is a special one. As is seen in the inset, the position of the main peak $T_{\max}$ moves to lower $T/[S(S+1)]$ as S increases from $1/2$ to 2 and all approaches yield almost identical predictions for that. When S exceeds 2, the main peak continues to decrease, however, the predictions of different methods become quite different. Similar picture occurs for the height of the main peak $c(T_{\max})$, see the main panel.

In summary, we may conclude that an extra low-temperature feature below the main maximum of $c(T)$ is present for $S = 1/2$, 1, $3/2$ only, but not for larger spin values $S \geq 5/2$. Some observed features are similar to those obtained by the RGM calculations of $c(T)$ and $\chi(T)$ for the spin-S KHAF [53]. For example, according to Ref. [53], the position of the main maximum of $c(T)$ shifts towards lower values of $T/(S(S+1))$ with increase of S, however, the role of low-lying excitations relevant for the low-temperature physics is beyond the RGM approach.

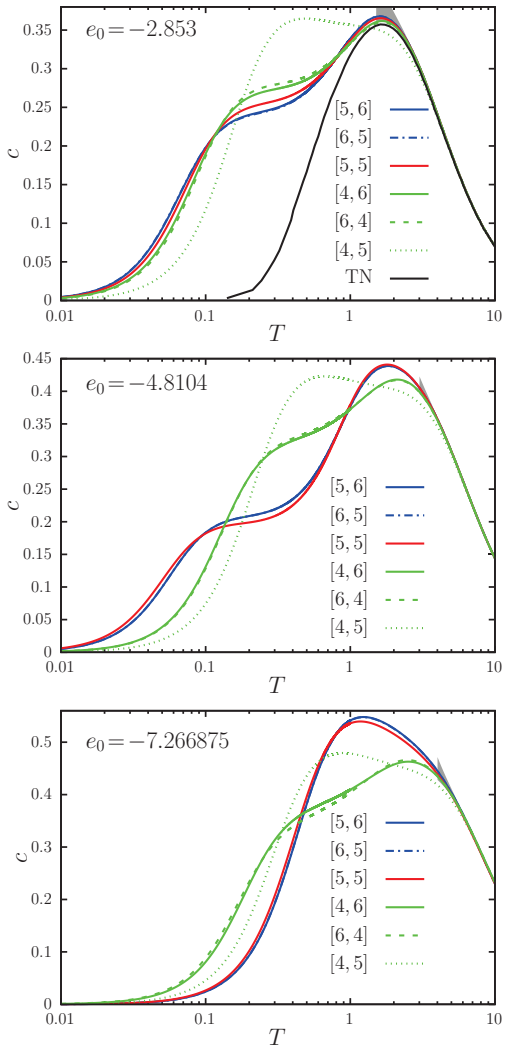

Figure 4. $c(T)$ for the spin-S KHAF within the entropy method for (top) $S = 3/2$, (middle) $S = 2$, and (bottom) $S = 5/2$. In the panel with $S = 3/2$ data we also plot the tensor-network result of Ref. [17].

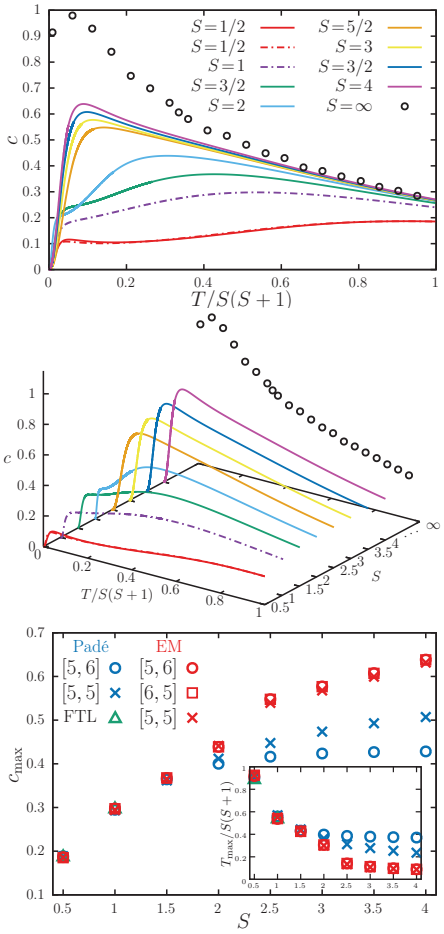

Figure 5. Top and middle panels: $c(T)$ for the spin-S KHAF within the entropy method (Padé approximant $[5,6](e)$ only). The values of e_0 were taken from the CCM paper [5]. Solid lines correspond to the assumption about the gapless spectrum with $\alpha = 2$; dash-dotted lines (for $S = 1/2$, 1) correspond to the assumption about the gapped spectrum. Classical Monte Carlo data [18] are shown by circles. Bottom panel: Main maximum of the specific heat $c_{\max} = c(T_{\max})$ of the spin-S KHAF obtained by various methods (entropy method, simple Padé approximation and numerics for $N = 42$, $S = 1/2$ [27] and $N = 21$, $S = 1$). Main panel: $c_{\max}$ versus S. Inset: $T_{\max}$ versus S.

4. Summary

The main challenge in describing the thermodynamics of the spin-S KHAF is a lack of appropriate methods for calculation of thermodynamic quantities for the whole temperature range. HTE augmented by the entropy-method seems to be a possible tool to tackle the problem. In the present paper, we have illustrated a crossover between pure quantum (small S) and classical (large S) behavior of the specific heat of the spin-S KHAF: The low-temperature feature of the specific heat (shoulder) disappears as S exceeds a specific value, the value of which according to our calculations is 2.

It is worth to mention a recent theory of a hidden energy scale, which is significantly lower than the microscopic energy scale of spin interactions, presented in Refs. [69, 70]. The hidden energy scale manifests itself as a lower-temperature peak, well below the common higher-temperature peak, in $c(T)$. With our study we may put forward a question about the role of the spin value S in this scenario for the hidden energy scale for geometrically frustrated magnets.

Acknowledgments

This preprint is a part of ongoing research launched several years ago by a team which includes Taras Hutak (L'viv), Johannes Richter (Magdeburg), Andreas Hauser (Magdeburg), Patrick Müller (Magdeburg), Heinz-Jürgen Schmidt (Osnabrück), Jürgen Schnack (Bielefeld), Taras Krokhmalskii (L'viv), and Oleg Derzhko (L'viv). O. D. acknowledges the kind hospitality of the MPIPKS, Dresden in September-November of 2019. T. H., T. K., and O. D. are thankful to the Armed Forces of Ukraine for protection since 2014, and especially since February 24, 2022. This project is funded by the National Research Foundation of Ukraine (2023.03/0063, Frustrated quantum magnets under various external conditions).

Supplemental Material

A: The ground-state energy for the $S = 1$ and $S = 3/2$ cases

In Table 1 and Table 2 we collected the ground-state energies obtained by various authors for the case $S = 1$ and $S = 3/2$, respectively. The CCM ground-state energy for $S = 2$, 5/2, 3 can be found in Ref. [5],

Table 1. The ground-state energy per site e_0 for the $S = 1$ KHAF obtained by various methods [exact diagonalization (ED) for various clusters of $N = 18$ sites and $N = 24$, series expansion (SE) method assuming $\sqrt{3}\times\sqrt{3}$ or q=0 order, nonperturbative linked-cluster expansion (NLCE), density-matrix renormalization-group (DMRG) algorithm, tensor-network (TN) methods, coupled-cluster method (CCM) assuming $\sqrt{3}\times\sqrt{3}$ or q=0 order, hexagonal singlet solid (HSS) state, resonating Affleck-Kennedy-Lieb-Tasaki loop (RAL) state, triangular valence-bond solid (TVBS) state].

	e_0/S^2 $(S=1)$
ED	$-1.451\,10$ (N=18a), $-1.439\,26$ (N=18b) [10]; $-1.426\,689\,4$ (N=24) [11]
SE	$-1.395\,0$ ($\sqrt{3}\times\sqrt{3}$), $-1.390\,3$ (q=0) [15]
NLCE	$-1.411\,4$ [14]
DMRG	$-1.410(2)$ [10]; $-1.411\,1$, $-1.412\,2$ [13]
TN	$-1.411\,6(4)$ [8]
CCM	$-1.403\,1$ ($\sqrt{3}\times\sqrt{3}$), $-1.396\,5$ (q=0) [5]
HSS	-1.36 [10]; $-1.360\,0$ [12]; $-1.410\,95$ [13]
RAL	-1.383 [6]
TVBS	$-1.387\,1$ [12]; $-1.391\,2 \pm 0.002\,5$ [13]; -1.40 [15]

Table 2. The ground-state energy per site e_0 for the $S = 3/2$ KHAF obtained by various methods [series expansion (SE) method, tensor-network (TN) methods, coupled-cluster method (CCM)].

	e_0/S^2 $(S=3/2)$
SE	-1.2530 ($\sqrt{3}\times\sqrt{3}$), -1.2527 (q=0) [15]
TN	$-1.265(2)$ [17]
CCM	-1.2680 ($\sqrt{3}\times\sqrt{3}$), -1.2643 (q=0) [5]

whereas the CCM data for $S = 7/2$ and $S = 4$ are $e_0 = -13.677\,125$ and $e_0 = -17.649\,269\,368\,7$, respectively. Concerning the opposite limit of infinite temperature, HTE up to 10th order for arbitrary spin S can be found in Appendix B of Ref. [65].

It might be interesting to illustrate the consistency of the low- and high-temperature properties of the KHAF using the sum rules for the internal energy and the entropy,

$$e(T)-e_0 = \int_0^T \mathrm{d}T c(T); \quad e_0 = -\int_0^\infty \mathrm{d}T c(T) \tag{A1}$$

and

$$s(T)= \int_0^T \mathrm{d}T \frac{c(T)}{T}; \quad \ln 2= \int_0^\infty \mathrm{d}T \frac{c(T)}{T}, \tag{A2}$$

see Ref. [19]. Replacing $c(T)$ by a simple Padé approximant, e.g., $[5,6](T)$ and the lower limit in the integrals $T = 0$ by a value T^* until which all Padé approximants agree with each other, we can estimate the upper bound e_0^* for e_0 and a part of the entropy, which comes from the temperature region $[0, T^*]$. One more estimate for e_0 may be obtained as in Ref. [71], Supplemental Material, Appendix D (this approach uses a monotonous decrease of $e(T)$ as T decreases to zero).

B: HTE for $S = 2,\ 5/2,\ 3,\ 7/2,\ 4$

Here, we report the 11th order coefficients in HTE for the KHAF with $S = 2,\ 5/2,\ 3,\ 7/2,\ 4$. We have

$$\begin{aligned} d_{11} &= -\frac{625\,587\,268\,339}{151\,200} J^{11}, \\ c_{11} &= \frac{2\,863\,397\,370\,551}{1\,260\,000} J^{10} \end{aligned} \tag{B1}$$

for $S = 2$,

$$\begin{aligned} d_{11} &= \frac{10\,417\,179\,602\,755\,425\,863}{15\,479\,341\,056} J^{11}, \\ c_{11} &= \frac{17\,166\,356\,000\,458\,470\,419}{77\,396\,705\,280} J^{10} \end{aligned} \tag{B2}$$

for $S = 5/2$,

$$d_{11} = \frac{90\,425\,361\,936\,437}{2\,520} J^{11},$$
$$c_{11} = \frac{7\,229\,967\,967\,257\,239}{793\,800} J^{10} \tag{B3}$$

for $S = 3$,

$$d_{11} = \frac{1\,708\,825\,945\,895\,179\,243}{1\,966\,080} J^{11},$$
$$c_{11} = \frac{3\,104\,351\,513\,640\,540\,433}{14\,745\,600} J^{10} \tag{B4}$$

for $S = 7/2$, and

$$d_{11} = \frac{44\,103\,941\,566\,868\,273\,233}{3\,306\,744} J^{11},$$
$$c_{11} = \frac{53\,216\,684\,483\,872\,733\,269}{16\,533\,720} J^{10} \tag{B5}$$

for $S = 4$.

C: Entropy-method interpolation

In the entropy method, we pass to the microcanonical ensemble working with the entropy (per site) s as a function of the energy (per site) e, $s(e)$, in the whole (finite) range of energies. The temperature T and the specific heat (per site) c are given by the formulas

$$T = \frac{1}{s'}, \quad c = -\frac{s'^2}{s''}, \tag{C1}$$

where the prime denotes the derivative with respect to e. These equations form a parametric representation of the dependence $c(T)$. Knowing the high-temperature series for $c(T)$ up to nth order we immediately get the series for $s(e)$ around $e = e_\infty = 0$ up to the same order n,

$$s(e)|_{e\to e_\infty=0} \to \ln(2S+1) + \sum_{i=2}^{n} a_i e^i, \tag{C2}$$

the coefficients a_i are the known functions of the coefficients d_i, see Appendix A of Ref. [56]. The behavior of $s(e)$ as e approaches the ground-state energy e_0 is also known. It is,

$$s(e)|_{e\to e_0} \propto (e-e_0)^{\frac{\alpha}{1+\alpha}} \tag{C3}$$

if $c(T)$ vanishes as T^α when $T \to 0$ (gapless excitations) and

$$s(e)|_{e\to e_0} \propto -\frac{e-e_0}{\Delta}\left(\ln\left[\Delta\,(e-e_0)\right]-1\right) \tag{C4}$$

if $c(T)$ vanishes as $T^{-\alpha}\exp(-\Delta/T)$, $\alpha = 2$ when $T \to 0$ (gapped excitations). Therefore we proceed differently in the gapless case and in the gapped case. Here it is assumed that e_0 and α are known (gapless case) or e_0 is known and $\alpha = 2$ (gapped case).

In the gapless case, we introduce the auxiliary function [23]

$$G(e) = \frac{(s(e))^{\frac{1+\alpha}{\alpha}}}{e-e_0} \tag{C5}$$

and approximate it as follows

$$G_{\rm app}(e) = G(0)[u,d](e), \quad G(0) = \frac{[\ln(2S+1)]^{\frac{1+\alpha}{\alpha}}}{-e_0}, \tag{C6}$$

where $[u,d](e) = P_u(e)/Q_d(e)$ denotes the Padé approximant and the coefficients of the polynomials $P_u(e)$ and $Q_d(e)$ (of order u and d, respectively, $u+d \le n$) are determined by the condition that the expansion of $[u,d](e)$ has to agree with the power series of $G(e)/G(0)$ [which follows from Eqs. (C5) and (C2)] up to order $\mathcal{O}(e^{u+d})$. Of course, $G(0) = G_{\rm app}(0)$. The approximate entropy follows by inverting Eq. (C5)

$$s_{\rm app}(e) = \left[(e-e_0)\,G_{\rm app}(e)\right]^{\frac{\alpha}{1+\alpha}}. \tag{C7}$$

The approximate prefactor A in the power-law decay of the specific heat $c(T)$ for $T \to 0$, $c(T) \to AT^\alpha$, is given by

$$A_{\rm app} = \frac{\alpha^{1+\alpha}}{(1+\alpha)^\alpha}\left[G_{\rm app}(e_0)\right]^\alpha. \tag{C8}$$

In the gapped case, we introduce the auxiliary function [56]

$$G(e) = (e-e_0)\left(\frac{s(e)}{e-e_0}\right)' \tag{C9}$$

and approximate it as follows

$$G_{\rm app}(e) = G(0)[u,d](e), \quad G(0) = \frac{\ln(2S+1)}{e_0}, \tag{C10}$$

where $[u,d](e) = P_u(e)/Q_d(e)$ again denotes the Padé approximant and the coefficients of the polynomials $P_u(e)$ and $Q_d(e)$ (of order u and d,

respectively, $u+d \le n$) are determined by the condition that the expansion of $[u,d](e)$ has to agree with the power series of $G(e)/G(0)$ [which follows now from Eqs. (C9) and (C2)] up to order $\mathcal{O}(e^{u+d})$. Of course, $G(0) = G_{\rm app}(0)$. The approximate entropy follows by inverting Eq. (C9)

$$\frac{s_{\rm app}(e)}{e-e_0} = \frac{\ln(2S+1)}{-e_0} - \int\limits_{e_0 \le e \le 0}^{0} {\rm d}\xi \frac{G_{\rm app}(\xi)}{\xi - e_0}. \tag{C11}$$

From technical point of view, before performing the integration in the r.h.s. of Eq. (C11) we have to perform the partial fraction expansion of the integrand which is obviously a rational function. The approximate energy gap Δ in the decay of the specific heat $c(T)$ for $T \to 0$, $c(T) \propto T^{-2}\exp(-\Delta/T)$, is given by

$$\Delta_{\rm app} = -\frac{1}{G_{\rm app}(e_0)}. \tag{C12}$$

Until now we assumed that there is no external magnetic field. In the presence of the magnetic field h, we face the entropy $s(e,h)$. The magnetization (per site) m and the magnetic uniform susceptibility (per site) χ are given by the formulas [29]

$$m = \frac{1}{(s(e,h))'}\frac{\partial s(e,h)}{\partial h}, \quad \chi = \frac{m}{h}; \tag{C13}$$

the last equation implies that h is infinitesimally small. Clearly, in the presence of (infinitesimally small, in practice, sufficiently small, say, $10^{-10}\ldots 10^{-3}$: One decreases h until the result does not further vary) fixed magnetic field h the HTE coefficients for the specific heat are changed,

$$d_i \to d_i + \frac{(i-1)i}{2}c_{i-1}h^2, \quad i = 2,\ldots,n, \tag{C14}$$

and we again arrive at Eq. (C2) in which the coefficients a_i are now the known functions of the coefficients d_i, c_i, and h. For the gapless case all reasonings in Eqs. (C3), (C5) to (C8) hold with the only difference: The ground-state energy now is $e_0 - \chi_0 h^2/2$, where χ_0 is the ground-state susceptibility which is assumed to be known. The obtained in Eq. (C7) entropy depends now on h, $s_{\rm app}(e,h)$. For the gapped case the ground-state energy remains unchanged in the presence of infinitesimally small magnetic field, i.e., $\chi_0 = 0$, and therefore all reasonings in Eqs. (C4), (C9) to (C12) hold. Again, the obtained in Eq. (C11) entropy depends now on h, $s_{\rm app}(e,h)$.

In summary, knowing the high-temperature $c(T)$ and $\chi(T)$ together with the ground-state energy e_0, the exponent α, and the ground-state susceptibility χ_0 (gapless case) or the ground-state energy e_0 (gapped case, $\alpha = 2$) we obtain $c(T)$ and $\chi(T)$ at all temperatures. [$s_{\rm app}(e,h)$ yields the specific heat $c(T)$ by Eq. (C1) and the susceptibility $\chi(T)$ by Eqs. (C13) and (C1)]. Usually, those Padé approximants which give unphysical solutions are discarded; the remaining ones are called "physical" [23, 56]. However, one may use even the unphysical Padé approximants after putting the Padé approximants with "defects" in the proper perspective [62, 68].

The authors of the recent paper [29] have demonstrated that even if the ground-sate energy e_0 is unknown (very often it is the case), it can be extracted from the rest available information based on the idea that larger is number of coinciding Padé approximants, best is estimation for e_0. In the present study, we use e_0 as an input even though the exact e_0 values for $S \ge 1/2$ remain unknown.

Finally, we mention the logZ-method interpolation. The logZ method is another scheme for interpolating with constraints [58]. Within this method one works in the canonical ensemble only and the method is applicable for finite systems too. We consider the function

$$l(\beta,h) = \frac{\ln Z(\beta,h,N)}{N} = -\beta f(T,h), \tag{C15}$$

which gives the specific heat $c(T,h)$ or the uniform susceptibility $\chi(T,h)$,

$$c(T,h) = \beta^2\frac{\partial^2 l(\beta,h)}{\partial\beta^2}, \quad \chi(T,h) = \frac{1}{\beta}\frac{\partial^2 l(\beta,h)}{\partial h^2}. \tag{C16}$$

We know the high-temperature behavior of $l(\beta,h)$, see Eq. (2). Moreover, in some cases we know the low-temperature behavior detailedly. For instance, for finite systems we have

$$\ln Z(\beta,0,N) \overset{\beta\to\infty}{\to} -\beta E_0 + \mathsf{d}_1\exp(-\beta\Delta E_1) + \ldots, \tag{C17}$$

where E_0 is the ground-state energy, $\Delta E_1 = E_1 - E_0$, E_1 is the first-excited-state energy and d_1 is its degeneracy and even more excited states can be taken into account. Then we may write [58]

$$l_{\rm app}(\beta,0) = -\beta e_0 + \frac{\mathsf{d}_1\exp(-\beta\Delta E_1)+\ldots}{N}\frac{\sum_{n=0}^{6}\mathsf{a}_n\beta^n}{1+\sum_{n=1}^{5}\mathsf{a}_{n+6}\beta^n + \mathsf{a}_6\beta^6} \tag{C18}$$

and determine the Padé coefficients $\mathsf{a}_0, \ldots, \mathsf{a}_{11}$ using the high-temperature series for $l(\beta, 0)$ up to order $n = 11$. In the presence of magnetic fields, taking into account that the states may experience the Zeeman splitting, one may construct $l_{\rm app}(\beta, h)$. While the specific heat for finite systems within the logZ method was discussed in Ref. [58], the susceptibility has not been studied within this approach so far.

D: Entropy-method calculations for the square-lattice $S = 1/2$ and $S = 1$ Heisenberg antiferromagnets

The problems with $\chi(T)$ within the entropy method may be illustrated using as a testing bed the square-lattice $S = 1/2$ or $S = 1$ Heisenberg

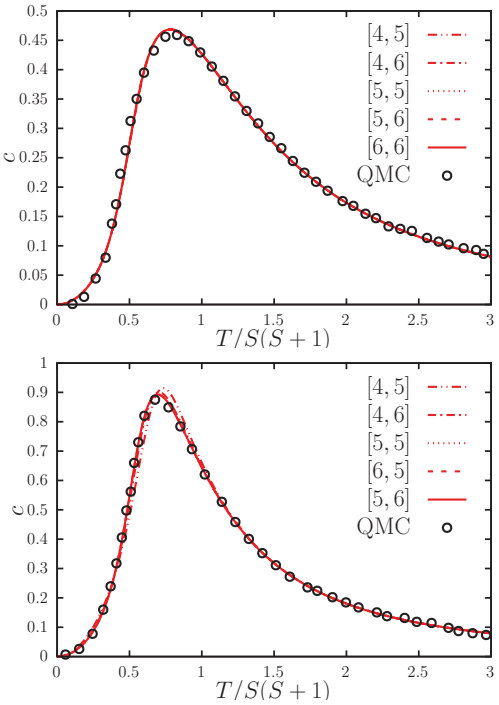

Figure 6. Specific heat $c(T)$ for the square-lattice Heisenberg antiferromagnet with spin (top) $S = 1/2$ and (bottom) $S = 1$ within the entropy method. Circles correspond to quantum Monte Carlo data [72].

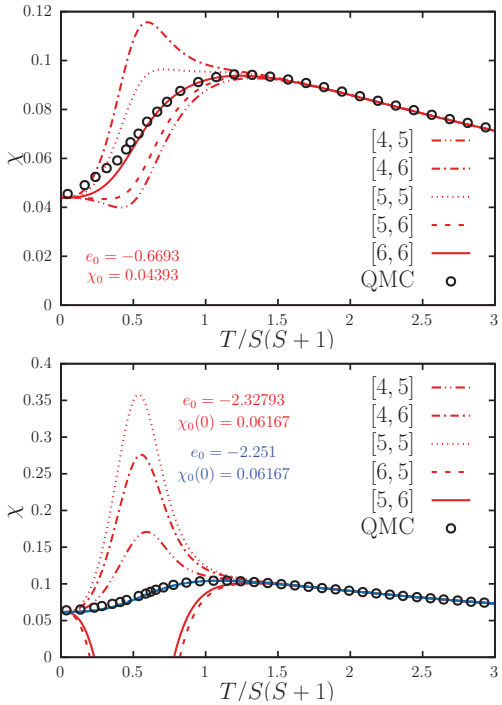

Figure 7. Susceptibility $\chi(T)$ for the square-lattice Heisenberg antiferromagnet with spin (top) $S = 1/2$ and (bottom) $S = 1$ within the entropy method. Circles correspond to quantum Monte Carlo data [72].

antiferromagnet. Reliable quantum Monte Carlo (QMC) data exist and they can be used for comparison. To apply the entropy method, we take into account that the energy spectrum is gapless, the exponent for power-law decay of $c(T)$ as $T \to 0$ is $\alpha = 2$, and the values of e_0 and χ_0 may be taken from Ref. [73]. Our findings are presented in Figs. 6 and 7.

As can be seen in these figures, the entropy method is able to reproduce QMC data for the specific heat for $S = 1/2$ and $S = 1$ (Fig. 6), but is less reliable for the susceptibility, especially when $S = 1$ (Fig. 7). Interestingly, by increase e_0 by $\approx 3.3\%$ ($-2.327\,93 \to -2.251$) one gets the blue curves in the lower panel of Fig. 7, which are much closer to QMC data. However, for the correct value of e_0, the entropy method predicts incorrect temperature shapes of the susceptibility, see the red curves in the lower panel of Fig. 7.

A general message that may be derived from this example as well as from another example discussed in Sec. 3.1 is that the entropy method works better for the specific heat than for the susceptibility. We may also mention here the entropy-method results for $\chi(T)$ of the $S = 1/2$ KHAF [29] and the numerical results of Refs. [27, 30] which poorly agree this way indicating that a reliable calculation of $\chi(T)$ for frustrated quantum spin systems remains an open problem.

To end up, we note that the square-lattice spin-S Heisenberg antiferromagnet may be an interesting nonfrustrated model for checking how the temperature dependence of the specific heat $c(T)$ (obtained by the entropy method and compared to QMC data) varies as the spin quantum number S grows. To obtain such results, which are similar to those in Fig. 5, we need HTE series for $S = 3/2$, 2, 5/2, 3, 7/2, 4; they can be obtained up to $n = 11$ using the Magdeburg code [64, 65]. Comparing two lattices, the kagome lattice and the square lattice, from the perspective of Fig. 5 may be an interesting task for future studies which allows to compare and contrast the frustrated and nonfrustrated lattices, both with the coordination number 4.

References

1. C. Lacroix, P. Mendels, and F. Mila, *Introduction to Frustrated Magnetism: Materials, Experiments, Theory*, Springer Series in Solid-State Sciences (Springer Berlin Heidelberg, 2011).
2. K. Hida, Journal of the Physical Society of Japan **69**, 4003 (2000).
3. K. Hida, Journal of the Physical Society of Japan **70**, 3673 (2001).
4. Z. Cai, S. Chen, and Y. Wang, Journal of Physics: Condensed Matter **21**, 456009 (2009).
5. O. Götze, D. J. J. Farnell, R. F. Bishop, P. H. Y. Li, and J. Richter, Phys. Rev. B **84**, 224428 (2011).
6. W. Li, S. Yang, M. Cheng, Z.-X. Liu, and H.-H. Tu, Phys. Rev. B **89**, 174411 (2014).
7. T. Picot and D. Poilblanc, Phys. Rev. B **91**, 064415 (2015).
8. T. Liu, W. Li, A. Weichselbaum, J. von Delft, and G. Su, Phys. Rev. B **91**, 060403 (2015).
9. O. Götze and J. Richter, Phys. Rev. B **91**, 104402 (2015).
10. H. J. Changlani and A. M. Läuchli, Phys. Rev. B **91**, 100407 (2015).
11. H. Nakano and T. Sakai, Journal of the Physical Society of Japan **84**, 063705 (2015).
12. W. Li, A. Weichselbaum, J. von Delft, and H.-H. Tu, Phys. Rev. B **91**, 224414 (2015).

13. S. Nishimoto and M. Nakamura, Phys. Rev. B **92**, 140412 (2015).
14. D. Ixert, T. Tischler, and K. P. Schmidt, Phys. Rev. B **92**, 174422 (2015).
15. J. Oitmaa and R. R. P. Singh, Phys. Rev. B **93**, 014424 (2016).
16. T. Picot, M. Ziegler, R. Orús, and D. Poilblanc, Phys. Rev. B **93**, 060407 (2016).
17. T. Liu, W. Li, and G. Su, Phys. Rev. E **94**, 032114 (2016).
18. J. T. Chalker, P. C. W. Holdsworth, and E. F. Shender, Phys. Rev. Lett. **68**, 855 (1992).
19. N. Elstner and A. P. Young, Phys. Rev. B **50**, 6871 (1994).
20. T. Nakamura and S. Miyashita, Phys. Rev. B **52**, 9174 (1995).
21. P. Tomczak and J. Richter, Phys. Rev. B **54**, 9004 (1996).
22. P. Sindzingre, G. Misguich, C. Lhuillier, B. Bernu, L. Pierre, C. Waldtmann, and H.-U. Everts, Phys. Rev. Lett. **84**, 2953 (2000).
23. G. Misguich and B. Bernu, Phys. Rev. B **71**, 014417 (2005).
24. M. Rigol, T. Bryant, and R. R. P. Singh, Phys. Rev. Lett. **97**, 187202 (2006).
25. M. Rigol, T. Bryant, and R. R. P. Singh, Phys. Rev. E **75**, 061118 (2007).
26. T. Shimokawa and H. Kawamura, Journal of the Physical Society of Japan **85**, 113702 (2016).
27. J. Schnack, J. Schulenburg, and J. Richter, Phys. Rev. B **98**, 094423 (2018).
28. X. Chen, S.-J. Ran, T. Liu, C. Peng, Y.-Z. Huang, and G. Su, Science Bulletin **63**, 1545 (2018).
29. B. Bernu, L. Pierre, K. Essafi, and L. Messio, Phys. Rev. B **101**, 140403 (2020).
30. C. Hotta and K. Asano, Phys. Rev. B **98**, 140405 (2018).
31. A. J. García-Adeva and D. L. Huber, Phys. Rev. B **63**, 140404 (2001).
32. M. E. Zhitomirsky, Phys. Rev. Lett. **88**, 057204 (2002).
33. M. R. Norman, Rev. Mod. Phys. **88**, 041002 (2016).
34. P. Mendels and F. Bert, Comptes Rendus. Physique **17**, 455 (2016).
35. Q. Barthélemy, A. Demuer, C. Marcenat, T. Klein, B. Bernu, L. Messio, M. Velázquez, E. Kermarrec, F. Bert, and P. Mendels, Phys. Rev. X **12**, 011014 (2022).
36. K. Awaga, T. Okuno, A. Yamaguchi, M. Hasegawa, T. Inabe, Y. Maruyama, and N. Wada, Phys. Rev. B **49**, 3975 (1994).
37. N. Wada, T. Kobayashi, H. Yano, T. Okuno, A. Yamaguchi, and K. Awaga, J. Phys. Soc. Jpn. **66**, 961 (1997).
38. I. Watanabe, N. Wada, H. Yano, T. Okuno, K. Awaga, S. Ohira,

K. Nishiyama, and K. Nagamine, Phys. Rev. B **58**, 2438 (1998).
39. D. Papoutsakis, D. Grohol, and D. G. Nocera, Journal of the American Chemical Society **124**, 2647 (2002).
40. G. Lawes, M. Kenzelmann, N. Rogado, K. H. Kim, G. A. Jorge, R. J. Cava, A. Aharony, O. Entin-Wohlman, A. B. Harris, T. Yildirim, Q. Z. Huang, S. Park, C. Broholm, and A. P. Ramirez, Phys. Rev. Lett. **93**, 247201 (2004).
41. J. N. Behera and C. N. R. Rao, Journal of the American Chemical Society **128**, 9334 (2006).
42. T. Matsushita, N. Hamaguchi, K. Shimizu, N. Wada, W. Fujita, K. Awaga, A. Yamaguchi, and H. Ishimoto, Journal of the Physical Society of Japan **79**, 093701 (2010).
43. W. Miiller, M. Christensen, A. Khan, N. Sharma, R. B. Macquart, M. Avdeev, G. J. McIntyre, R. O. Piltz, and C. D. Ling, Chemistry of Materials **23**, 1315 (2011).
44. D. E. Freedman, R. Chisnell, T. M. McQueen, Y. S. Lee, C. Payen, and D. G. Nocera, Chem. Commun. **48**, 64 (2012).
45. S. Hara, H. Sato, and Y. Narumi, Journal of the Physical Society of Japan **81**, 073707 (2012).
46. E. T. Connolly, P. Reeves, D. Boldrin, and A. S. Wills, Journal of Physics: Condensed Matter **30**, 025801 (2017).
47. H. J. Silverstein, R. Sinclair, A. Sharma, Y. Qiu, I. Heinmaa, A. Leitmäe, C. R. Wiebe, R. Stern, and H. Zhou, Phys. Rev. Mater. **2**, 044006 (2018).
48. I. S. Hagemann, Q. Huang, X. P. A. Gao, A. P. Ramirez, and R. J. Cava, Phys. Rev. Lett. **86**, 894 (2001).
49. D. Bono, P. Mendels, G. Collin, N. Blanchard, F. Bert, A. Amato, C. Baines, and A. D. Hillier, Phys. Rev. Lett. **93**, 187201 (2004).
50. B. Fåk, F. C. Coomer, A. Harrison, D. Visser, and M. E. Zhitomirsky, Europhysics Letters **81**, 17006 (2007).
51. K. Okuta, S. Hara, H. Sato, Y. Narumi, and K. Kindo, Journal of the Physical Society of Japan **80**, 063703 (2011).
52. S. Okubo, R. Nakata, S. Ikeda, N. Takahashi, T. Sakurai, W.-M. Zhang, H. Ohta, T. Shimokawa, T. Sakai, K. Okuta, S. Hara, and H. Sato, Journal of the Physical Society of Japan **86**, 024703 (2017).
53. P. Müller, A. Zander, and J. Richter, Phys. Rev. B **98**, 024414 (2018).
54. A. M. Läuchli, J. Sudan, and E. S. Sørensen, Phys. Rev. B **83**, 212401 (2011).
55. A. M. Läuchli, J. Sudan, and R. Moessner, Phys. Rev. B **100**, 155142 (2019).
56. B. Bernu and G. Misguich, Phys. Rev. B **63**, 134409 (2001).

57. B. Bernu and C. Lhuillier, Phys. Rev. Lett. **114**, 057201 (2015).
58. H.-J. Schmidt, A. Hauser, A. Lohmann, and J. Richter, Phys. Rev. E **95**, 042110 (2017).
59. O. Derzhko, T. Hutak, T. Krokhmalskii, J. Schnack, and J. Richter, Phys. Rev. B **101**, 174426 (2020).
60. V. Grison, P. Viot, B. Bernu, and L. Messio, Phys. Rev. B **102**, 214424 (2020).
61. M. G. Gonzalez, B. Bernu, L. Pierre, and L. Messio, SciPost Phys. **12**, 112 (2022).
62. T. Hutak, T. Krokhmalskii, O. Derzhko, and J. Richter, The European Physical Journal B **96**, 50 (2023).
63. T. Hutak, T. Krokhmalskii, J. Schnack, J. Richter, and O. Derzhko, Phys. Rev. B **110**, 054428 (2024).
64. H.-J. Schmidt, A. Lohmann, and J. Richter, Phys. Rev. B **84**, 104443 (2011).
65. A. Lohmann, H.-J. Schmidt, and J. Richter, Phys. Rev. B **89**, 014415 (2014).
66. L. Pierre, B. Bernu, and L. Messio, SciPost Phys. **17**, 105 (2024).
67. M. E. Zhitomirsky, Phys. Rev. B **78**, 094423 (2008).
68. G. A. Baker and P. Graves-Morris, *Padé Approximants* (Cambridge University Press, 1996).
69. P. Popp, A. P. Ramirez, and S. Syzranov, Origin of the hidden energy scale and the f-ratio in geometrically frustrated magnets (2024), arXiv:2406.12966 [cond-mat.str-el] .
70. A. P. Ramirez and S. Syzranov, Order and disorder in geometrically frustrated magnets (2024), arXiv:2408.16054 [cond-mat.str-el] .
71. I. Hagymási, R. Schäfer, R. Moessner, and D. J. Luitz, Phys. Rev. Lett. **126**, 117204 (2021).
72. D. C. Johnston, R. J. McQueeney, B. Lake, A. Honecker, M. E. Zhitomirsky, R. Nath, Y. Furukawa, V. P. Antropov, and Y. Singh, Phys. Rev. B **84**, 094445 (2011).
73. C. J. Hamer, Z. Weihong, and P. Arndt, Phys. Rev. B **46**, 6276 (1992).